Progress In Electromagnetics Research, Vol. 140, 681–717, 2013

THE DESIGN OF AN OPTICAL TIME STEERED ANTENNA BASED ON A NEW INTEGRATED TRUE TIME DELAY UNIT

Amedeo Capozzoli, Claudio Curcio, and Giuseppe D'Elia*

Dipartimento di Ingegneria Elettronica e delle Telecomunicazioni, Università degli Studi di Napoli Federico II, Via Claudio 21, Napoli 80125, Italia

Abstract—In the framework of wide-band and ultra wide-band array antennas, an Optical Time Steered Antenna (OTSA) is presented, by considering the design strategies of a new True Time Delay (TTD) Control Unit in the Beam Forming Network (BFN). The unit has high reliability, low crosstalk, low switching time and potential low cost, being based on a low cost technology. Furthermore, due to its compactness and modularity, it can be easily grouped with other ones to make a control unit of large arrays. Different strategies and working configurations of the TTD control unit are presented as a trade-off among hardware complexity, insertion loss reduction and beam control capability. The design of an OTSA prototype is discussed by considering a realistic model simulating the behavior of a real world antenna and accounting for unavoidable non-realities, such as random, periodic and systematic errors introduced by each device exploited in the OTSA as well as mutual coupling between radiating elements. An optimal trimming strategy, able to compensate at best for BFN errors and based on the use of suitably located trimmers, is presented. Among other cases, to enlighten the potentialities of the OTSA, an all optical architecture providing a difference beam squint free pattern is also proposed.

1. INTRODUCTION

The current and future communication systems will require reliable and low cost innovative antenna systems, with advanced features such as high spatial scan coverage, high scanning resolution, small beam

Received 15 August 2012, Accepted 12 November 2012, Scheduled 28 June 2013

* Corresponding author: Giuseppe D'Elia (g.delia@unina.it).

scanning times, fine sidelobe control, wide or ultrawide bandwidth, beam squint free steering, independent control of multiple beams [1]. On the other hand, some physical and environmental specifications are also required: reduced size and weight, interference immunity, transportability, antenna conformability to a given geometry, wide operating temperature range, mechanical reliability.

Array antennas represent an attractive solution to attain the above requirements, since, thanks to their discrete nature, they can realize advanced beam control features, such as fine and flexible beam shaping, fast beam steering, multiple simultaneous beams and flexible null positioning.

The design of the array is usually performed by applying a strategy composed of three steps.

The first step is external synthesis. In particular, the technology of the radiating elements is defined, by also considering their electromagnetic characteristics. The main geometrical parameters are fixed, and the excitation coefficients of the array elements are determined by applying a synthesis algorithm accounting also for physical constraints such as those related to quantization and finite dynamic.

As the second step, the design of the BFN is afforded. Firstly, the BFN technology is chosen, then the network configuration is selected (according to the BFN requirements) and, finally, the BFN is designed, to provide the excitation coefficients prescribed by the external synthesis, thanks also to an optimization process of the quality parameters of the network.

In the third step, an accurate modeling of the array is exploited to forecast the electromagnetic behavior of the whole antenna system and, to refine the results of the design procedure, allowing a finer tuning of the available parameters.

In this paper, we consider the design of the BFN for wideband steered arrays providing the advanced beam features considered above.

To attain a wideband (beam-squint free) steering, the BFN is designed by exploiting the TTD principle [2], and the phase shifter approach must be avoided. However, because the conventional microwave technology leads to bulk, heavy and complex BFN's, especially in the case of large arrays, alternative technologies have been proposed to realize compact and lightweight BFN's for wide band applications [2].

A promising solution is represented by the optical technology [3–7]. Indeed, optics allows to naturally implement the TTD principle, thus realizing ultra-wide band beam-squint free phased arrays with high interference immunity, low size and weight BFN's.

Following a widespread classification, the most promising approaches to realize variable optical time delays can be grouped in two main categories: the Switched Delay Lines (SDL) and the Variable Propagation Velocity Lines (VPVL) [7–9].

With the SDL approach, the required time delay is obtained by driving the light selectively into fibers with appropriate lengths. To this end, optical or electrical switches can be employed. The delay stages, made by the switch and the delay lines, can be, essentially, arranged in serial or parallel configurations [3, 4]. A classical SDL series architecture is the binary fiber optic delay line discussed in [4, 10] which employs optical switches and fiber segments whose length increases progressively by a power of 2. A parallel SDL implementation has been presented in [11], where a set of electrical switches has been used to select the laser source coupled with the fiber of proper length. Such a structure has been employed in the first demonstration of a wide band beam-squint free system driving an array of 8 elements, made of 4 subarrays of two elements each, operating in the band $1.9\,\text{GHz} \div 9\,\text{GHz}$.

In the VPVL approach, the time delay of the optical signal is changed by varying its propagation velocity [12]. This can be achieved by means of tunable lasers feeding high dispersion fibers [13], or fiber Bragg gratings [14]. The fiber dispersion prism architecture has been proved in different practical realizations for 1D and 2D arrays [13, 15, 16]. Moreover, another interesting wavelength-selective architecture, proposed in [17], is based on the spectral periodicity of arrayed waveguide gratings arranged on a recirculating configuration. The VPVL approach allows the continuous beam-steering. Recent examples of photonic TTD control can be found in [18–23].

The aim of this paper is twofold.

The first is to show the potentialities of the integrated optical TTD unit presented in [24], called TTDU later on. It is an integrated device, based on the SDL scheme, compact and very flexible, whose performance compared to those of competitor SDL's are summarized in [25].

The unit can be used in different working configurations allowing a convenient trade-off among hardware complexity, insertion loss and beam control capabilities. The basic TTDU exploited here allows driving up to 8 radiating elements in the frequency range 5–30 GHz. It is modular, since different TTDU's can be easily grouped together, on the one hand to build control units of larger and larger arrays, and, on the other hand, to improve the driving performances of the BFN for a fixed array dimension. Then, the design of an Optical Time Steered Antenna (OTSA) based on such a TTDU is presented, discussing in detail, given the design guidelines for an OTSA, all the relevant aspects:

a. Features and working configurations of the proposed TTDU;
b. Array design and evaluation of beam capabilities of an OTSA based on the proposed TTDU;
c. Full modeling of an OTSA based on the proposed TTDU and its performance evaluation;
d. Trimming strategy of an OTSA based on the proposed TTDU.

The guidelines to design the OTSA are presented in Section 2. They will be used to define the antenna architecture, and then, to determine the time delay performance required to the proposed optical time delay network (the TTDU) given the array configuration, or to define the array configuration and the corresponding beam capabilities, given the time delays distribution.

The features of the TTDU are briefly reported in Section 3, while the considered TTDU working configurations are presented in Section 4.

The array design and the evaluation of the beam capabilities, corresponding to different TTDU working configurations, are discussed in Section 5, according to the guidelines in Section 2.

To make effective the OTSA design and correctly evaluate the achievable performance, the behavior of the whole antenna system is realistically simulated by using commercial optical and radiofrequency (RF) software packages (see Section 6). This approach makes possible to take into account for the unavoidable non-idealities affecting the optical/RF devices, as random, periodic and systematic errors.

The OTSA modeling has been exploited in Section 6 to evaluate the impact of the random errors on the antenna performance. Concerning the systematic errors, a trimming strategy has been proposed in Section 7, to compensate for them, improving, on average, the antenna response under all the working configurations (e.g., different beam pointing directions). In Section 7, thanks to the OTSA modeling, the effectiveness of the trimming strategy has been evaluated.

Finally, in Section 8, the second aim of the paper is presented: to design an OTSA radiating sum and difference beam squint free patterns. This concept has been validated, again thanks to the OTSA modeling, and the results are presented once again in Section 8.

Conclusions are drawn in Section 9.

2. THE OTSA DESIGN GUIDELINES

In this section, the guidelines for the design of an OTSA are given in terms of specifications for the optical time delay network, for an

assigned array configuration, or in terms of the array specification for a given optical time delay system.

The general layout of the OTSA is depicted in Fig. 1. The generation and modulation section (block a)) provides the light signals needed to feed the optical BFN, properly modulated by the RF source. The light signals enter block b), the TTD control unit, which provides as many signals as the number of array elements, with the time delays distribution corresponding to the desired beam steering angle. The optical signals are then down converted to RF within block c), providing the microwave signals needed to drive the radiating system (block d)).

Later on, we will call the system made by blocks a), b) and c) as Time Phaser (TPH).

The TTD control unit is the core of the TPH. Designing the TTD control unit represents a key task of the whole OTSA design. In fact, for a given radiating system, the beam steering control features of the OTSA strictly depend on the time delay distribution achievable with the control unit. Moreover, the design of the stages a) and c) depends on the TTD control unit structure.

Once the OTSA scheme has been defined by referring to a TTD control unit based on a M-bits SDL scheme (since the TTDU belongs to such a class), we can identify the design guidelines as:

I. Choice of the antenna feeding architecture: Array/Sub-Array;

II. Choice of the maximum time delay $\tau_{\max}$;

III. Choice of the number M of bits (time delay quantization);

IV. Practical issues.

Points I and IV have already been discussed in [25]. Here we summarize the design formulas related to the maximum time delay $\tau_{\max}$ and spend some words regarding the time delay quantization. These two aspects will become relevant in the next sections of the present paper.

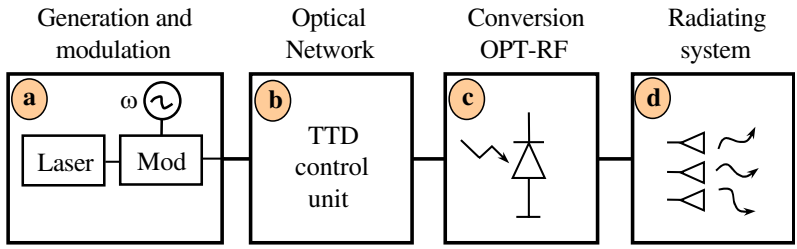

Figure 1. Layout of the OTSA based on the TTDU.

An M bits SDL time shifter provides $2^M - 1$ delays, namely $0,\ \tau_e,\ 2\tau_e, \ldots, (2^M - 1)\tau_e$, multiples of an elementary one, say τ_e, giving a maximum achievable time delay $\tau_{\max} = (2^M - 1)\tau_e$. As discussed in [25], for a linear array of N elements/subarrays, with uniform spacing d, radiating a beam pointing at an angle θ with respect to the normal to the array, the value for $\tau_{\max}$ is related to the desired maximum beam pointing angle $\theta_{\max}$ and to the radiating system aperture $A = (N-1)d$ by the equation:

$$|\tau_{\max}| = \frac{A}{c} sen\,|\theta_{\max}| = \frac{(N-1)d_\lambda}{f_D} \sin|\theta_{\max}| \tag{1}$$

where c is the light speed in the vacuum, f_D the nominal RF working frequency, and $d_\lambda = d/\lambda_D$ the inter-element distance normalized to the wavelength $\lambda_D = c/f_D$. According to (1), to achieve the desired $\theta_{\max}$, the TPH, for a given array length A, must provide a $\tau_{\max}$ given by (1). On the other hand, a given TPH, with a maximum delay $\tau_{\max}$, allows the beam steering of an antenna with aperture A up to the angle $\theta_{\max}$ given by (1).

Regarding the number M of quantization bits, it must be noted that a high value for M, although reducing the time delay quantization error, also increases hardware complexity and losses. In fact, larger quantization levels require larger numbers of delay stages, thus increasing the total losses and hardware complexity of each time shifter, as discussed in [25, 26].

For an M bits time shifter, the time delay error is uniformly distributed across a time interval equal to τ_e. Accordingly, the related error on the phase of the excitation coefficient φ_{err} is given by [27]:

$$|\varphi_{err}| = \left|\frac{\omega\tau_e}{2\sqrt{3}}\right| = \left|\frac{\pi f \tau_{\max}}{\sqrt{3}\,(2^M - 1)}\right| \tag{2}$$

where f is the microwave operating frequency.

Here we are mainly interested in highlighting the effects on the pattern degradation, such as finite beam steering resolution and sidelobe level raising. Moreover, when dealing with subarray structures, the phase error due to the finite bandwidth of the RF signal must be also considered [2]. Indeed, changing the working frequency introduces a squint of the subarray pattern so that undesired grating lobes are introduced [2].

In particular, the choice of the minimum number M of quantization bits should account for the acceptable values for the beam steering resolution $\Delta\theta$, the peak (QL_{peak}) and the average side lobe

level (σ^2_{Tavg}), as shown in [2]:

$$\Delta\theta = \frac{c\tau}{L\cos\theta_0} = \frac{c\tau_{\max}}{L\cos\theta_0\,(2^M-1)} \tag{3}$$

$$QL_{\text{peak}}(\text{dB}) = 3.92 + 20\log\left(\frac{f\tau_{\max}}{2^B-1}\right) \tag{4}$$

$$\sigma^2_{\text{Tavg}} = \frac{1}{3D}\frac{(\pi f\tau_{\max})^2}{(2^B-1)^2} \tag{5}$$

Concerning the beam pointing resolution, Matthews [8], in the case of a subarray structure and a broadside beam pointing configuration, suggests as an acceptable beam pointing resolution that equal to one half of the 3 dB beam-width. Accordingly, for an array with aperture A, the number M of bits is given by:

$$M \approx 3.322\log\left(\frac{2.257A}{\lambda}\right) \tag{6}$$

3. THE NEW TTD UNIT

As discussed in the Introduction, the BFN of the steered array will be designed by exploiting the TTD unit, called TTDU, discussed in this section.

The TTDU is based on the innovative cross-connect switch presented in [28, 29] and realizes a switched delay line matrix. The chip, whose layout is represented in Fig. 2, is made by 2 sets of H integrated optical waveguides intersecting at $H \times H$ cross points (the black dots in Fig. 2). Furthermore, the TTDU allows other interesting features such as high reliability, low crosstalk, low switching time (< 1 ms), and

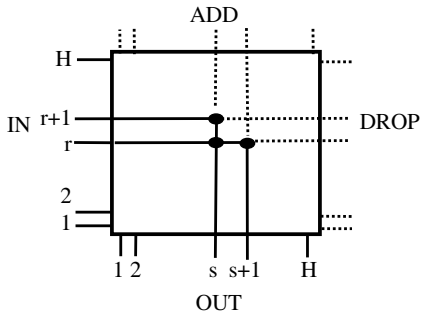

Figure 2. The TTDU layout.

a potential low cost, since it is based on a low cost technology, the one used for inkjet thermal actuators [29, 30].

Let us denote with r and s, $r = 1, \ldots, H$ and $s = 1, \ldots, H$, the indexes of the generic input and output port of the switch, respectively. At each cross point a trench is etched and filled with a fluid whose refractive index is matched to the waveguide. The switching of the light beam entering the r-th waveguide towards the s-th output is made possible by generating a small bubble at the corresponding cross point, by means of a thermal actuator based on the inkjet technology. Since the bubble displaces the liquid, the light beam is reflected toward the crossing waveguide [28, 29].

Obviously, the delay of the light signal entering the r-th input is due to the optical path corresponding to the switched configuration and can be easily changed by activating a different cross point. On the other hand, if no cross points are activated, the light entering the r-th input waveguide passes through the TTDU and arrives at the r-th "drop" port (Fig. 2). The "drop" ports together with the "add" ports allow to realize modular structures wherein, by arranging together several basic units, a larger cross connect switch with higher available delay times can be obtained. On the other hand, the TTDU allows a bidirectional driving strategy.

To drive a phased array antenna, the input-output relationships of the TTDU, in terms of delays and insertion losses, must be specified. In particular, the delay τ associated to the input-output pair (r, s) is given by:

$$\tau\ (r, s) = \tau_{\text{ref}} + (r - 1)\,\tau_{\Delta} + (s - 1)\,\tau_{\Delta} \tag{7}$$

where τ_{ref} (equal to zero later on) is the reference delay accounting for both the delay on the input path between the chip connector and the first input crosspoint plus the delay between the last crosspoint and the output chip connector on the output path, while τ_{Δ} is the elementary delay between two adjacent cross points.

The TTDU losses L can be expressed as (see Fig. 2):

$$L\,(r, s) = 2C + R + (r - 1)T + (s - 1)T \tag{8}$$

where C is the loss due to the path between the chip input (output) connector and the first (last) cross point of the chip, T is the loss due to propagation between two consecutive cross points and R is the loss related to the reflection at the cross point.

Following [27, 28] we assume, $\tau_{\Delta} = 1.5\,\text{ps}$, $C = 0.25\,\text{dB}$, $T = 0.07\,\text{dB}$ and $R = 2.1\,\text{dB}$.

It is stressed that according to Eqs. (7) and (8), different delays are associated to different signal losses.

4. THE TTDU DRIVING STRATEGIES

In this section, several TTDU driving strategies and the related TPH configurations are discussed.

The strategies have been devised to optimize the trade-off between the TTDU time steering control capabilities and the antenna apparatus requirements. Concerning the time steering control, different approaches have been studied in order to drive antennas with different characteristics, such as the number and the spacing of the radiating elements, the working frequency and beam scanning resolution. Concerning the antenna apparatus requirements, the TTDU configurations leading at compact BFNs, with reduced hardware complexity, high reliability and reduced insertion losses have been considered. To reduce the hardware complexity and costs, driving strategies allowing to drive several radiating elements at the same time with a single TTDU have been introduced.

In the following, we refer to an OTSA driven by a 32×32 TTDU.

Two different driving modalities have been considered:

- agile beam control (M BITS mode);
- staring beam control (K BEAM mode).

In the first case, an M bits time shifter providing the desired time delay distribution needed to control a "continuous" beam steering (apart from quantization errors) is designed, for each radiating element. In the staring beam case, the TTDU has been designed to furnish only the time delays set needed to obtain K fixed beam configurations.

Before we discuss the different working configurations, some observations are in order.

Let us consider the case of a TTDU implementing N time shifters, driving N radiating elements. For each time shifter, the set of input-output pairs (r, s) corresponding to the desired delays must be identified. They will be denoted in the following as active inputs and active outputs, respectively. Accordingly, section a) of the OTSA must be designed in order to feed all the TTDU active inputs, while section c) must drive the delayed signals available at the TTDU active outputs to the corresponding radiating elements (see Fig. 1).

Concerning the design of the block a), to reduce hardware complexity, a configuration based on a single laser, a single high speed modulator and a star coupler feeding all the TTDU active inputs has been considered. The use of an integrated star coupler, allows a very compact input section. For what concerns the design of the block c), a configuration using a photodetector for each time shifter has been considered. In this way, as it will be seen, star couplers driving the TTDU active outputs to the corresponding photodetector are needed.

Each star coupler introduces a signal loss, growing with the number of coupled inputs, which must be taken into account when designing the working configurations.

Designing section c), two possibilities are of concern. In the first one, a set of contiguous outputs are assigned to the time shifters so that integrated star couplers can be used to increase compactness and reliability. On the contrary, when not contiguous output ports are considered, fiber couplers are needed. It will be shown later on that, although this solution provides non compact output stages, it could be more convenient since it allows a better time delay performance.

The different TTDU driving configurations are described in [24]. Two simple configurations (3 and 5 BITS) based on mono-directional driving have been reported in [25], while here we will consider a 3 BEAM strategy and a 5 BITS configuration, the latter based on a bidirectional driving:

1) 3 BEAM — 6 elements — Contiguous outputs;
2) 5 BITS — 4 elements (bidirectional driving) — Contiguous outputs.

The first one has been considered to give an example of a 6 elements time steered antenna radiating 3 beams.

Regarding the 5 BITS configuration the solution here presented, at difference of that in [25] which provides wider time delay ranges useful to drive large antennas with subarray architectures, exploits a bidirectional driving of the TTDU allowing an integrated and very compact structure, since it requires the minimum amount of external delays. Furthermore, it generates a small delay range, up to several tenths of picoseconds, well suited to drive antennas working in the microwave range.

4.1. The 3 BEAM — 6 Elements Configuration

In this simple configuration, the TTDU is required to provide the time delay distributions needed to steer the beam of a six elements antenna towards 3 different directions, say $\theta_1 = 0$, $\theta_2 = \theta_A$, $\theta_3 = -\theta_A$. Three sets of 6 time delays are required, according to Table 1, where the delay distribution needed to radiate the broadside beam has been set constant (see row 1 of Table 1), while the delay distributions needed to radiate the two steered beams have been properly chosen to get the corresponding positive and negative slopes (see rows 2 and 3, respectively, of Table 1).

To radiate the broadside beam, all time shifters are set to provide the same time delay equal to Δt. As it will be clearer later on in this section, this choice reduces the delay range required by the 2nd, 3rd,

4th and 5th time shifters in the non broadside cases, thus reducing the number of the required TTDU outputs and, as a consequence, the BFN losses due to the star couplers required in block c).

The maximum delay generated by the time shifters is $\tau_{\max} = 5\Delta t$ (see Table 1).

Aim of the design procedure is to define the TTDU input-output pairs which, at the same time, give the time delays in Table 1 and maximize the achievable $\tau_{\max}$ while using a minimum number of TTDU inputs and outputs.

To get a compact BFN we will refer to a contiguous output grouping criterion: the intervals of output, assigned to each time shifter, do not overlap.

First, it is necessary to identify the input-output pairs related to the minimum and maximum delays, i.e., τ_0 and $\tau_{\max}$, respectively.

To get a wide $\tau_{\max}$, the input-output pairs related to τ_0 and $\tau_{\max}$ must be located as far as possible from each other. Since only the 1st and 6th time shifters must provide these two delays (see Table 1), and only four elements remain to be fed, it is worth to assign to the 1st shifter the outputs from 1 to 15 and to the 6th shifter the outputs from 20 to 32. As far as the other shifters are concerned, we will assign them only one TTDU output. In order to reduce the signal losses, the 2nd uses the output 16, the 3rd the output 17, the 4th the output 18, and the 5th the output 19, as shown in Fig. 3, wherein the working scheme of the 3 BEAM — 6 elements mode is schematically depicted. Stage a) is connected, by means of a coupler, to the TTDU inputs. TTDU areas assigned to each time shifter are identified by vertical dash-dot lines, and the TTDU outputs are connected to the photodetectors feeding the 6 radiating elements of the array, exploiting couplers, when needed.

When choosing the input-output pairs for the 1st and 6th elements, it must be noted that, as seen from Table 1, they have the same (reversed) time delay range.

Let us first define the input-output pairs for the 6th time shifter.

The maximum delay in the 6th time shifter is obtained when the input-output pairs (1, 20) and (32, 32) are used, providing the delays

Table 1. Time delay for the 3 BEAM — 6 elements mode.

	Time shifter					
Beam	**1**	**2**	**3**	**4**	**5**	**6**
$\theta_1 = 0°$	Δt	Δt	Δt	Δt	Δt	Δt
$\theta_2 = \theta_A$	0	Δt	$2\Delta t$	$3\Delta t$	$4\Delta t$	$5\Delta t$
$\theta_3 = -\theta_A$	$5\Delta t$	$4\Delta t$	$3\Delta t$	$2\Delta t$	Δt	0

$\tau(1,20) = \tau_0$ and $\tau(32,32)$, respectively. With this choice we would have:

$$\tau_{\max} = \tau(32,32) - \tau(1,20) = 43\tau_\Delta = 64.5\,\text{ps} \tag{9}$$

However, because $\tau_{\max} = 5\Delta t$, we have $\Delta t = \tau_{\max}/5 = 8.6\tau_\Delta$, i.e., Δt would not be an integer multiple of τ_Δ, so that above choice is not allowed. It is worth to choose the input-output pairs (1, 20) and (32, 29) providing $\tau_{\max} = 40\tau_\Delta = 60\,\text{ps}$ and $\Delta t = \tau_{\max}/5 = 8\tau_\Delta = 12\,\text{ps}$ (these pairs are represented, in Fig. 3, with a filled and an empty dots, respectively). Obviously, smaller values of $\tau_{\max}$ and Δt can be achieved. In particular, the minimum value for $\tau_{\max}$ is $5\tau_\Delta = 7.5\,\text{ps}$.

To have a time delay $\Delta t = 8\tau_\Delta$, the input-output pair (9, 20) is used, adding a delay equal to $8\tau_\Delta$ to the delay τ_0 corresponding to the pairs, (1, 20). With this choice the 6th time shifter exploits the same TTDU output for two beams. Accordingly, the input-output pairs of the 6th time shifter are (9, 20), (32, 29) and (1, 20) for a beam pointing toward θ_1, θ_2 and θ_3, respectively.

Once the choice of the input-output pairs for the 6th time shifter is made, the 1st time shifter input-output pairs (r, s) corresponding to the τ_0 and the $\tau_{\max}$ can be easily found.

First, once the τ_0 has been fixed, the pair needed to achieve τ_0 for the 1st time shifter should be (20, 1). It is noted that, because the outputs of the first shifter are now restricted from 1 to 15, the widest delay corresponds to the pair (32, 15) and would be $\tau(32,15) - \tau(20,1) = 26\tau_\Delta$, smaller than the one realized with the 6th time shifter. To circumvent this problem and to allow the 1st time shifter realizing a maximum delay equal to the one of the 6th time shifter, an external biasing delay line equal to $14\tau_\Delta$ is introduced on the output of the first time shifter as shown in Fig. 3. The zero delay, i.e., τ_0, is now obtained by choosing the (6, 1) input-output pair (filled dot in Fig. 3) while the time delay Δt is obtained by considering the input-output pair (14, 1). As for the 6th time shifter, this pair has been obtained from the corresponding τ_0 delay pair, (6, 1) by adding a delay equal to $\Delta t = 8\tau_\Delta$ with the aim of using the same TTDU output. Accordingly, the input-output pairs of the 1st time shifter are (14, 1), (6, 1) and (32, 15) for a beam pointing toward θ_1, θ_2 and θ_3, respectively. The longest delay corresponding to the input-output pair (32, 15) is marked with an empty dot in Fig. 3, highlighted by an arrow.

Regarding the other shifters, to reduce the delay range, we can employ a proper external biasing delay. In particular, we can use an external delay equal to $\Delta t = 8\tau_\Delta$ for the 2nd, 3rd, 4th and 5th time shifters. In this way, these shifters are "time biased" at the time delay Δt. However, it is noted that the zero delay of Table 1 corresponds to

the reference time τ_0, that can be obtained by any input-output pair $(r,\ s)$ such that $r + s = 21$. Accordingly, the 2nd, 3rd, 4th and 5th time shifters input-output pairs providing the delay Δt of Table 1 can be obtained according to the relationship $r + s = 21$, and are reported in Table 2. The corresponding input-output pairs are represented as filled dots in Fig. 3.

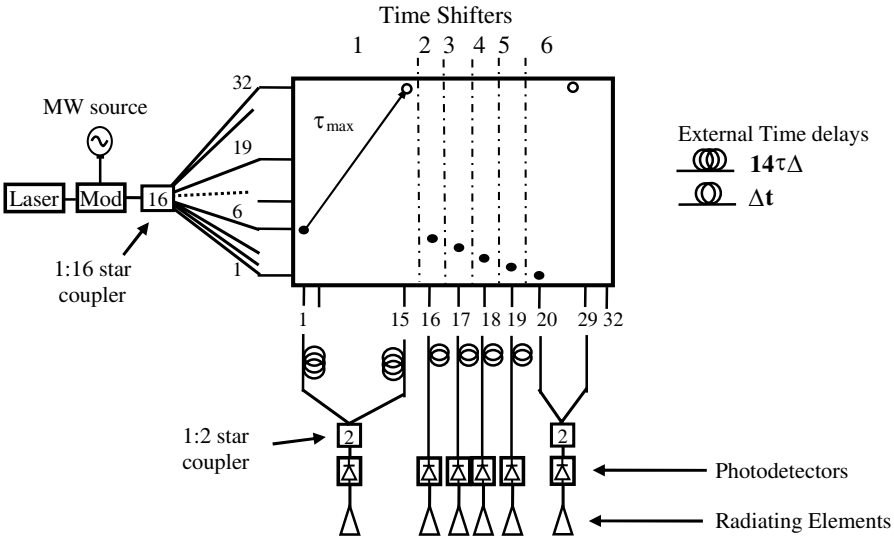

Figure 3. Working scheme of the 3 BEAM — 6 elements mode.

Finally, the other delays for the 2nd, 3rd, 4th and 5th time shifters are realized by changing the TTDU input index r, while keeping the same TTDU output index s for each time shifter.

The input-output pairs for each beam configuration are reported in Table 2.

Table 2. Input output pairs for the 3 BEAM – 6 elements mode.

	Time shifter					
Beam	**1**	**2**	**3**	**4**	**5**	**6**
$\theta_1 = 0°$	(14, 1)	(5, 16)	(4, 17)	(3, 18)	(2, 19)	(9, 20)
$\theta_2 = \theta_A$	(6, 1)	(5, 16)	(12, 17)	(19, 18)	(26, 19)	(32, 29)
$\theta_3 = -\theta_A$	(32, 15)	(29, 16)	(20, 17)	(11, 18)	(2, 19)	(1, 20)

This configuration exploits 15 TTDU inputs so that an 1 : 16 integrated star coupler can be used in stage a), with an insertion loss of about 12 dB. Accordingly the corresponding stage a) of the OTSA is obtained by a single laser, followed by a modulator and an 1 : 16 integrated star coupler, as shown in Fig. 3.

Regarding the outputs, the 1st and 6th time shifters use 2 outputs (see the 1 : 2 couplers followed by the photodetectors in stage c) depicted in Fig. 3), while the others employ only one output each. Accordingly, integrated combiners can be used to connect the time shifter outputs to the photodetectors. The insertion loss associated to the output combiners is at least equal to 3 dB for the 1st and 6th time shifters, while no combiner losses are associated to the other ones. Obviously, this insertion loss unbalance has to be properly compensated, as it will be shown in Section 7.

Thus, the worst insertion loss, apart from conversion losses and star coupler excess losses, involves the 1st and 6th time shifters, and is given by three main contributions: the insertion loss of the input combiner, the insertion loss due to the TTDU and the one due to the output combiner.

Here, for the sake of simplicity, but without losing generality, we neglect the connections losses and the losses due to the external delay lines, determining a systematic error to be compensated.

The BFN insertion loss IL_{BFN} is given by the TTDU loss term L associated to the input-output pairs (6, 1), according to the Eq. (5), and the insertion loss related to the input and output combiners. In particular, IL_{BFN} is given by:

$$\begin{aligned} IL_{\mathrm{BFN}}(\mathrm{dB}) &= IL_{\mathrm{inputcombiner}} + L(6,1) + IL_{\mathrm{outcombiner}} \\ &= 10\log 16 + (2C + R + 5T) + 10\log 2 \\ &\approx\ 12\,\mathrm{dB} + 3\,\mathrm{dB} + 3\,\mathrm{dB} \approx 18\,\mathrm{dB} \end{aligned} \tag{10}$$

On the other hand, the insertion loss related to the single time shifter IL_{T} must also be evaluated. It is given by IL_{BFN} minus the power division losses needed to feed the 6 radiating elements, which is equal to about 8 dB. Accordingly, the IL_{T} is about 10 dB.

Moreover, the insertion loss varies according to the considered input-output pairs. In particular, the maximum insertion loss variation due to the TTDU losses is referred in the following as the amplitude uniformity factor (AU), and in the steered beam configuration, related, for example, to the beam pointing angle θ_2, is given by:

$$\mathrm{AU} = L(32,29) - L(6,1) = 54T \approx 4\,\mathrm{dB} \tag{11}$$

4.2. The 5 BITS — 4 Elements Configuration: Bidirectional Driving

Thanks to the presence of "add" and "drop" ports, the TTDU can be driven in a bidirectional way, to improve the beam steering performance.

In this configuration, the left half side of the TTDU realizes two time shifters while the right half side realizes the remaining two ones (Fig. 4). Unlike the previous case, the scheme in Fig. 4 refers only to the TTDU. Again the TTDU areas assigned to each time shifter are identified by dash-dot lines. The exploited outputs are connected, through 8 : 1 couplers, to the photodetectors which are not explicitly shown.

Each side is again subdivided in two sections: the first 8 outputs are assigned to the 1st time shifter, while the outputs from 9 to 16 are

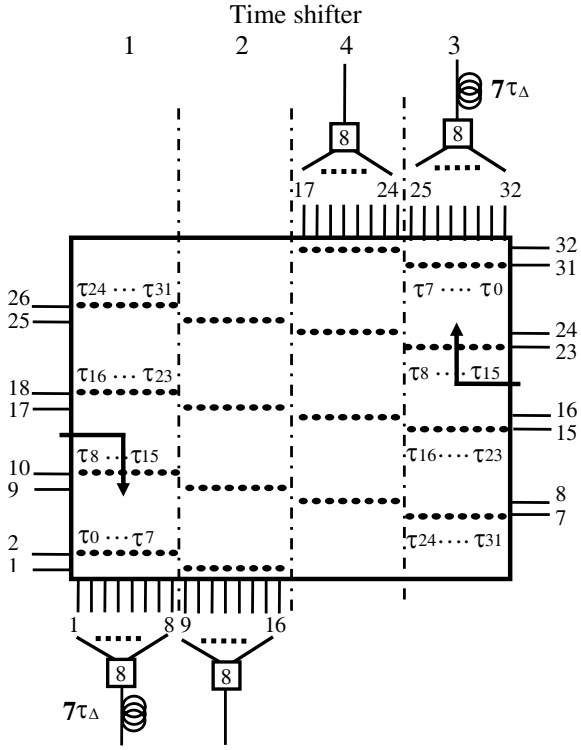

Figure 4. Working scheme in the 5 bit — 4 elements — Bidirectional driving mode.

assigned to the 2nd time shifter, to attain sets of contiguous outputs and realize a integrated and compact output stages. Accordingly, to achieve a 5 bits time shifter, the 32 input-output pairs exploit only 4 inputs and 8 outputs. In particular, we use $\Delta t = \tau_\Delta$ and $\tau_{\max} = 31\tau_\Delta = 46.5\,\text{ps}$. The input-output pairs related to the 1st and the 2nd time shifters are given by (filled dots in Fig. 4):

$$\begin{cases} r_\alpha = 2 + 8\lfloor n/8 \rfloor - (\alpha - 1) \\ s_\alpha = n + 1 - 8\lfloor n/8 \rfloor + 8(\alpha - 1) \end{cases} \tag{12}$$

with $\alpha = 1$, 2 and $n = 0, \ldots, 31$.

The input-output pairs related to the 3rd and 4th time shifters are given by (filled dots in Fig. 4):

$$\begin{cases} r_\alpha = 31 - 8\lfloor n/8 \rfloor + (\alpha - 3) \\ s_\alpha = 32 - n + 8\lfloor n/8 \rfloor - 8(\alpha - 3) \end{cases} \tag{13}$$

with $\alpha = 3$, 4 and $n = 0, \ldots, 31$.

External lines with delays of $7\tau_\Delta$, properly highlighted in Fig. 4, have to be used for the outputs involved by the 1st and the 3th time shifters.

This configuration requires a $1:16$ star coupler made of two $1:8$ couplers to feed the left and the right sides of the TTDU. Moreover, in the detection stage four $8:1$ output combiners are needed. The corresponding insertion loss is about 24 dB ($IL_{\text{T}} = 18\,\text{dB}$), while AU is about 2.5 dB.

The TTDU working scheme adopted for this case is depicted in Fig. 4.

5. DESIGN OF THE ARRAY AND EVALUATION OF THE BEAM CAPABILITIES

In this section, the guidelines for the array design are firstly given. In particular, to give an example, here we will refer to a printed linear array of N wideband elements (Strip-Slot-Foam-Inverted Patches (SSFIP) [24]), radiating a Tchebitchev pattern with 15 dB sidelobe level [31]. Obviously, the design approach is effective also for different array antennas. In the second part of this section the beam capabilities achievable in different TTDU driving configurations are evaluated, for a given array structure.

5.1. Array Design

To design the array, we will refer to the equations summarized in Section 2. In particular, for each TTDU working configuration, the

antenna aperture A must be fixed first. Since the number of radiating elements is assigned, the working frequency f_D and the normalized (to the wavelength $\lambda_D = c/f_D$) element spacing d_λ must be given.

Equation (1) is used to find f_D, once the maximum beam pointing angle $\theta_{\max}$ and d_λ are known. Conversely, if the f_D and d_λ are given, Eq. (1) provides the maximum achievable scanning range. Generally speaking, the maximum scanning angle $\theta_{\max}$ is chosen according to the application of interest (typical scanning ranges are $\theta_{\max} = \pm 45°$, or $\theta_{\max} = \pm 60°$ for wide scanning applications) while the spacing d_λ is chosen to avoid Grating Lobes (GL) and reduce mutual coupling effects.

For a quick and easy determination of either the frequency f_D or the scanning range $\theta_{\max}$, we introduced in [32] a planning chart representing $\tau_{\max}$ as function of $\theta_{\max}$ and the element spacing d_λ. The chart is reported in Fig. 5 in the case of a linear array of 4 radiating elements, for values of d_λ in the range $(0.5\lambda,\ 0.7\lambda)$, with a step equal to 0.05λ, and for three design frequencies f_D (10 GHz, 15 GHz, 20 GHz). According to the values of $\tau_{\max}$ obtained in the different TTDU working configurations, the planning chart allows to find the values of f_D and $\theta_{\max}$, once d_λ has been set.

Because GL's deteriorate the pattern shape, the chart highlights the set of values for d_λ which avoids GL's. With reference to the 3 BITS configuration, inserting in Eq. (1) the upper limit $d_0(\theta_{\max}) = 1/(\sin(\theta_{\max}) + 1)$, the curve $\tau_{\max} = \tau_{\max}(\theta_{\max})$ can be obtained and the corresponding GL's free zone, for each design frequency, can be sketched in the planning chart. In particular, in Fig. 5 the GL's free zones at 10 GHz, 15 GHz and 20 GHz are depicted.

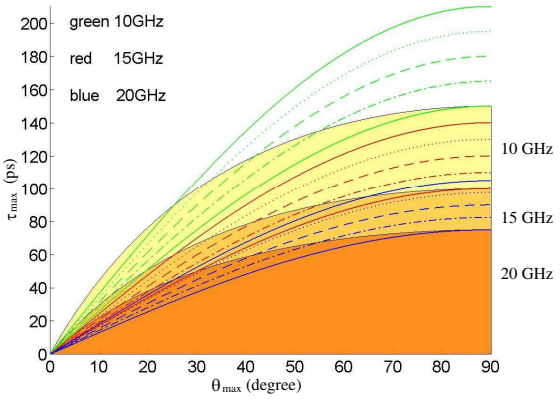

Figure 5. OTSA planning chart with the grating lobes free zones.

5.2. Evaluation of the Beam Capabilities

As far as the features of the radiated beam are concerned, in the K BEAM mode, only $\theta_{\max}$ must be considered, by using Eq. (1), while in the M BITS mode, also the time quantization effects must be evaluated, in terms of angular resolution $\Delta\theta$, quantization lobe peak (QL_{peak}) and average side lobe level (σ^2_{Tavg}) due to time delay quantization.

The beam capabilities attainable with all the TTDU configurations studied in [24] are reported in Table 3. In particular the label C refers to the contiguous output mode, while the label NC to the non contiguous outputs mode.

Table 3. Achievable beam features in the different TTDU working configurations.

K BEAM Mode					
Configuration	$\tau_{\max}$		f_D		
3 Beams 4 elements	67.5 ps		f_D~21 GHz		
3 Beams 6 elements	60 ps		f_D~39 GHz		
5 Beams 4 elements	63 ps		f_D~22 GHz		
M BITS Mode					
Configuration	$\tau_{\max}$	f_D	$\Delta\theta$	QL_{peak}	σ^2_{Tavg}
3 Bits 4 elements − C	52.5 ps	~26 GHz	~8°	~ −10 dB	~ −13 dB
3 Bits 4 elements −NC	94.5 ps	~15 GHz			
4 Bits 4 elements	202.5 ps	~7 GHz	~4°	~ −17 dB	~ − 19 dB
4 Bits 8 elements	180 ps	~18 GHz	~4°	~ −9 dB	~ − 15 dB
5 Bits 4 elements/subarrays	418.5 ps	4 elements array ~3 GHz	~2°	~ − 23 dB	~ − 26 dB
		4 subarrays (7 elements each) ~22 GHz			
5 Bits 4 elements Bidirectional	46.5 ps	~30 GHz			

For both the K BEAM and the M BITS mode, the values of f_D refers to a 60° scanning range. The values of QL_{peak} and σ^2_{Tavg} are referred to the worst case, using $f = f_D$. In particular, the value of σ^2_{Tavg} is raised by 2 dB to take into account for scan and taper losses [2].

Regarding the configuration 5 Bits — 4 elements, it can be used to feed an array or a sub-array structure. As an example, it could drive an array of 28 elements grouped into 4 sub-arrays of 7 elements half a wavelength spaced, working at $f_D = 22$ GHz, with a scanning range of 60°. Other array configurations are also possible [24].

6. OTSA MODELING

To make the OTSA design effective, the whole antenna apparatus has to be modelled to forecast, realistically, the response of the system.

To this end, it is crucial to have at disposal tools able to numerically simulate the entire system, made by the optical and the RF section. However, software able to describe both the optical circuit and the radiating elements are difficult to find. As a consequence, the two aspects must be dealt with by using two softwares, properly interfaced.

In principle, the photonic CAD should be able to simulate the chain realized by all the optical devices (laser, modulator, star couplers, combiners, photodetectors, fibers, connections, etc.) and at the same time it should allow to describe the functioning of the TTDU. On the other hand, the RF CAD should be used to evaluate the radiative and circuital behaviour of the radiating elements for all the required working configurations (different beam pointing directions). In particular, the circuital behaviour of the radiating elements can be exploited to evaluate (under the photonic CAD) the output signals, provided by the photodetectors. These signals can, then, be used, into the RF CAD, as excitations of the radiating elements to obtain the pattern evaluation.

To model the OTSA RF section we used the Ansoft Designer software, while to model the optical section of the OTSA we used the VPIphotonics. The two softwares have been interfaced by means of Python scripts. Python scripts have also been interfaced with Matlab, to obtain the antenna patterns reported in the following, and to perform the optimization described in Section 7.

In the following subsections, the modelling of both the radiating system and the TPH is described.

6.1. The Model of the Radiating System

Concerning the radiating system, since the behaviour of each radiating element can be easily evaluated by using electromagnetic CADs, only a modelling involving the circuital analysis of the antenna, accounting for the mutual coupling between the elements, has been considered.

Due to mutual coupling, the equivalent circuit of the array can be described using the concept of impedance matrix. Concerning the input of each element, the concept of active impedance must be exploited, whose values change according to the elemenst excitations, affecting the photodetectors performance employed in stage c) (see Fig. 1).

To highlight this point, the active impedances of the mentioned radiating system, a 4 elements printed linear array radiating a Tchebitchev pattern, has been numerically analysed by means of the EM simulator Ansoft Desinger by considering SSFIP patches, working at 18 GHz with a nominal input impedance equal to 100 Ω [24]. The active impedance (real and imaginary part) of the boundary element of the array is reported in Fig. 6 as a function of d_λ, for two different beam pointing angles: $\theta = 0$ and $\theta = 30°$.

As shown, the mutual coupling introduces a significant mismatch whose effects, for each beam pointing angle, can be reduced by a proper choice of d_λ. Unfortunately, the mismatch depends significantly on the beam pointing direction (Fig. 6).

Accordingly, to reduce the mismatching effects on the working of

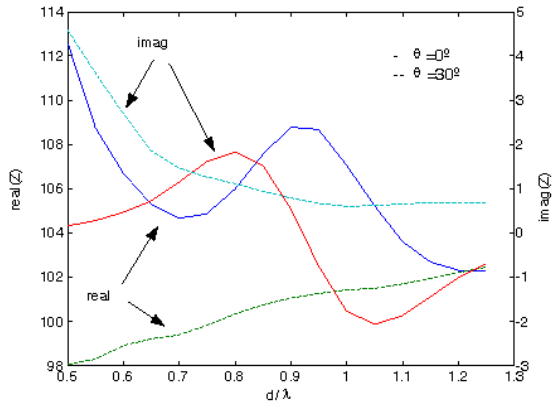

Figure 6. Active impedance of a boundary element versus d: Case $\theta = 0°$ and $\theta = 30°$.

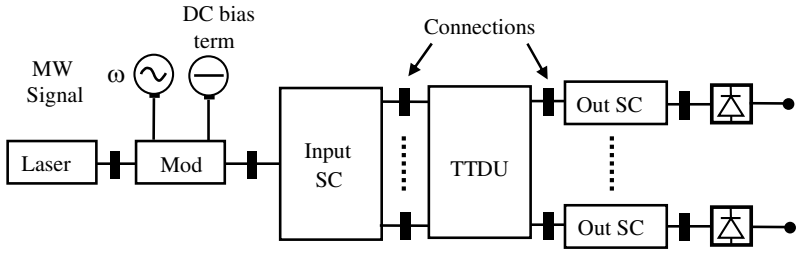

Figure 7. Model of time phaser.

the stage c), isolation stages become, or active broadband matching stages, between the optical and RF stage.

6.2. Time Phaser Model

The TPH model has been simulated by using the mentioned optical software.

The optical devices involved in the OTSA have been modelled by taking into account both the real characteristics of the commercial devices and the unavoidable realization defects which can introduce errors on the antenna excitations distribution.

The TPH model is schematically depicted in Fig. 7.

The main optical devices are the laser, modulator, TTDU, photodetectors, input and output star couplers/combiners and optical connections.

The laser source has been modelled as a module generating a continuous wave optical signal at the frequency Ω [Hz], with linewidth $\Delta\Omega$ [Hz], average power P_{LAS} [W], a given initial phase Φ_i [degree], a given Relative Intensity Noise (RIN) level [dB], measured at a given power level and a fixed polarization state.

The Mach-Zender Modulator (MZM), has been characterized by the $V_{\pi\mathrm{DC}}$ [V], the DC voltage required to realize a π phase difference, the $V_{\pi\mathrm{RF}}$ [V], the RF voltage required to realize the π phase difference, the insertion loss [dB] and the extinction ratio [dB] accounting for the real splitting ratio among the MZM arms.

The photodetector has been modelled as an envelope detector with bandwidth B [Hz] and responsivity r_{PD} [A/W]. Furthermore, the thermal, dark and shot noise processes have been characterized by the spectral density N_{TH} [A/Hz$^{0.5}$], and the current i_{PD} [A], the photodector output current [33].

The TTDU determines an attenuation and a programmable time delay on the optical signals, according to the working configuration

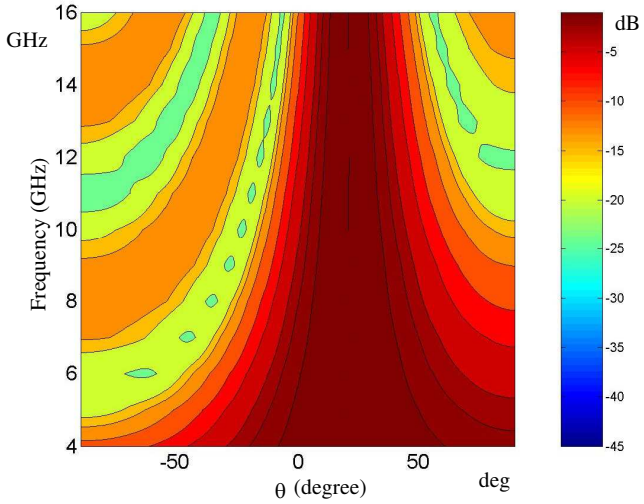

Figure 8. Array factor intensity as function of the angle θ and the frequency of the microwave signal achieved using the TPH model.

considered in Section 4, so that it can be modelled by referring to Eqs. (7) and (8).

Finally, the optical star coupler and combiners have been modelled as a stage with a given number N_{port} of inputs or outputs ports, with a known loss and time delay depending on N_{port}.

Obviously, the TPH model considered up to now has an ideal working. To verify what happens in these conditions, a linear array of 4 half a wavelength spaced elements, a fixed beam pointing angle equal to 20°, a nominal working frequency equal to 15 GHz, a 3 BITS — 4 elements TTDU working configuration and a microwave tone modulating the optical signal have been considered, and the noise sources have been neglected. The array factor of the antenna is shown under Fig. 8 as a function of both the observation angle and the frequency. As expected, a beam squint free pattern is obtained.

To have a real-world model, the unavoidable realization defects and their effects on the amplitude and time delay of the antenna excitations must be added.

In particular, let us consider the amplitude variations due to the realization defects (the time delay variation can be treated analogously).

Under high signal to noise ratio conditions, mainly the input and output star couplers, the connections and the TTDU affect the

amplitude distribution.

Following the results available in the literature, the star coupler/combiner insertion loss variations, can be described by a Gaussian distribution [34, 35]. Accordingly, the star couplers can be modeled as devices with a constant power loss, related to the number of outputs, plus a random insertion loss contribution with a Gaussian distribution on the available channels.

Analogously, the optical connections can be modelled by considering the insertion loss (dB) due to the connection plus a random term taking into account for the practical realization. In particular, a truncated Gaussian [35] or a Log-Normal [36] distribution can be used.

In a similar way, the realization defects of the TTDU can be taken into account by introducing random attenuation on the ports with a Gaussian distribution and a given standard deviation.

Accordingly, for a given TTDU working configuration, since all the losses can be modeled as independent Gaussian variables, the resulting insertion loss is Gaussian too. Furthermore, the mean value of the insertion loss of each time shifter is the sum of the means of the losses contributions due to the involved optical devices, while the variance is given by the sum of the variances.

In particular, the mean insertion loss IL_{mean} is given by:

$$IL_{\text{mean}}(r,s) = L(r,s) + IL_{\text{IN\_SC}} + IL_{\text{OUT\_CM}} + IL_{\text{conn}} \tag{14}$$

where the value of $L(r,s)$ is given by Eq. (8), $IL_{\text{IN\_SC}}$ is the mean value of the insertion loss related to the input star coupler, $IL_{\text{OUT\_CM}}$ is the mean insertion loss related to the output combiner, IL_{conn} is the mean value of the losses due to the all the connections.

Similarly, the loss variance σ^2_{IL} is given by:

$$\sigma^2_{IL} = \sigma^2_{IL\text{-TTDU}} + \sigma^2_{IL\text{-IN\_SC}} + \sigma^2_{IL\text{-OUT\_CM}} + \sigma^2_{IL\text{-Conn}} \tag{15}$$

where $\sigma^2_{IL\text{-TTDU}}$ is the variance related to the TTDU losses, $\sigma^2_{IL\text{-IN\_SC}}$ and $\sigma^2_{IL\text{-OUT\_CM}}$ are the variances related to the losses of the input and output couplers, respectively, and finally $\sigma^2_{IL\text{-Conn}}$ is the variance related to the connection losses.

According to these considerations, the optical devices employed in the OTSA must be properly designed to obtain a total loss deviation σ_{IL} below a given threshold error.

As an example, let us consider a 4 elements prototype, having a Tchebitchev nominal amplitude distribution with a -15 dB sidelobe level, a maximum tolerable sidelobe level variation equal to 5 dB, and a maximum tolerable beam pointing angle variation equal to 2°. Accordingly, a numerical analysis has been carried out to evaluate the acceptable amplitude and phase errors corresponding to the mentioned

pattern deterioration, by using as guidelines the results in the literature on the analysis of effects on the antenna pattern due to random errors on the antenna aperture distribution [2]. In particular, the amplitude and phase root mean square errors have been estimated to be equal to 0.82 dB and 5°, respectively [2, 37]. By using the modeling tool, the expected pattern deterioration has been verified by using the considered amplitude and phase error distribution within the TPH model.

7. ERROR COMPENSATION STRATEGY

Apart from the random errors due to realization defects, other sources of errors have to be taken into account when studying the antenna aperture distribution. These are periodic and systematic errors. The first ones are due to the quantization effects due to the use of digital time/phase shifters. The systematic errors are due to the losses within TTDU introduced above. The losses vary with the input-output pair (r, s) according to Eq. (8). As a consequence, the effects of these errors depend on the beam pointing configuration. Because such losses cause a serious deterioration of the beam nulls, an increase of the side lobe level and the broadening of the radiated beam, a compensation strategy is mandatory.

At variance of the random and periodic errors, which can be only statistically modelled, the systematic errors are accurately known so that a compensation strategy can be introduced already at the designing stage.

Losses compensation can be achieved by introducing trimming stages, which amplify or attenuate the light signal, within the BFN.

However, because the same TTDU input or output can be involved in different time shifters and the TTDU introduces different unbalances for each beam pointing configuration, losses compensation is not a trivial task. To obtain an efficient trimming strategy, for a given OTSA and a given set of beam pointing configurations, we have developed an evolutionary algorithm finding the number, the position and the trimming amount (attenuation or amplification) of the trimming stages ensuring the "best" reduction of the systematic errors effects, and providing an amplitude distribution as close as possible to the desired one.

As an example, a 4 bits — 4 elements working configuration [24] with a $\tau_{\max} = 90$ ps, working frequency equal to 15 GHz and a Tchebitchev amplitude distribution, allowing a -15 dB sidelobe level, has been considered. The input-output pairs and the insertion loss related to the TTDU are reported in Table 4, for three different

beam pointing angle: $\theta = 0°$, $\theta = \theta_{\max}$, $\theta = -\theta_{\max}$. As seen, no amplitude errors are reported in the broadside case, while the maximum unbalance between the 1st and the 4th element is obtained when considering the maximum scan angle.

The working scheme of the above configuration is schematically depicted in Fig. 9, showing the TTDU driving scheme, together with the trimming units, and the output stage. In this configuration, the TTDU drives 4 radiating elements, each one realizing a 4 bits time shifter. The needed 16 time delays use, for each time shifter, 4 TTDU outputs and 4 TTDU inputs. Since the outputs exploited for each

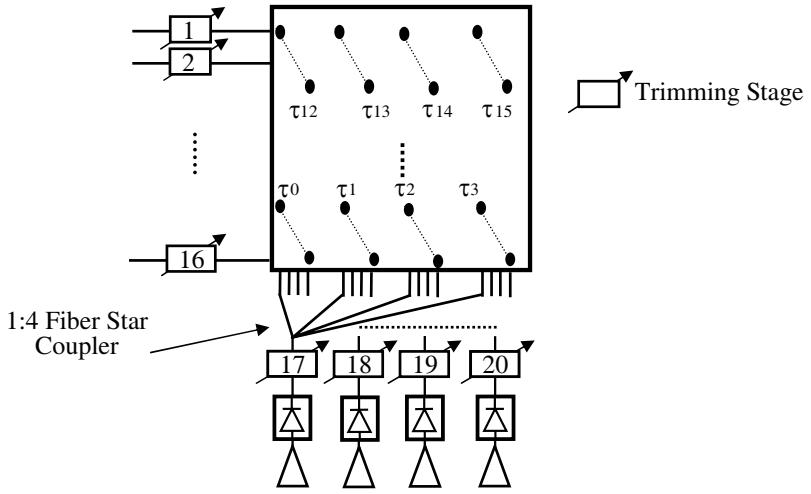

Figure 9. Trim stages configuration for the TTDU configuration 4 BIT — 4 elements — Non contiguous outputs mode.

Table 4. TTDU insertion loss and input-output pairs in the 4 bits — 4 elements working configuration.

	IL **(dB)** — (r, s)	
$\theta = 0°$	2.81 dB — (4,1)	2.81 dB — (3,2)
	2.81 dB — (2,3)	2.81 dB — (1,4)
$\theta = \theta_{\max}$	2.81 dB — (4,1)	4 dB — (11,11)
	5.19 dB — (18,21)	6.38 dB — (25,31)
$\theta = -\theta_{\max}$	6.38 dB — (28,28)	5.19 dB — (19,20)
	4 dB — (10,12)	2.81 dB — (1,4)

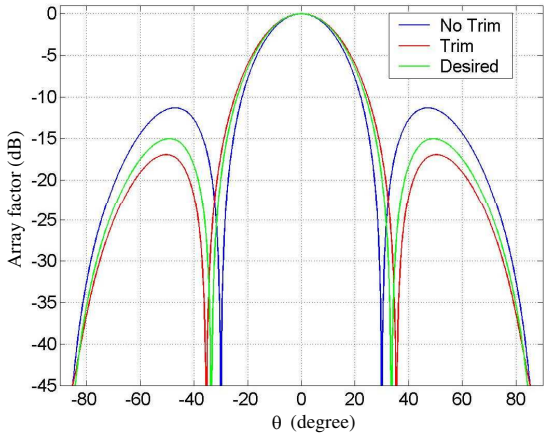

Figure 10. Comparison among the desired array factor and the one obtained with and without compensation: Broadside case ($\tau_{\max} = 90\,\text{ps}$).

time shifter are non contiguous, fiber star couplers should be adopted in this case (see Fig. 9). As in the previous schemes, the TTDU input-output pairs corresponding to a given delay are depicted as filled dots. However for the sake of simplicity, in Fig. 9, just a subset of the delay pairs is depicted: in particular, the depicted time delays are the first four (from τ_0 to τ_3) and the last four (from τ_{12} to τ_{15}).

In this configuration, the maximum number of trimming units is 20, as shown in Fig. 9. Indeed, 5 trimming units are adopted for each time shifter: one for each TTDU input (4 trimming units) and one after the fiber coupler collecting the four TTDU outputs. The optimization has been carried out for $K = 5$ beam pointing angles: $\theta_1 = 0°$, $\theta_{2,3} = \pm 20°$, $\theta_{4,5} = \pm 40°$.

In the optimization algorithm the modelling of the system has been obtained by using the mentioned tool realizing the synergy among Matlab, Pyton and VPIphotonics.

The considered evolutionary algorithm involved a population with $N_{\text{pop}} = 100$ individuals and a fitness function, say X, defined as the sum of the distances between the desired amplitude coefficients and the ones realized with the TTDU, for all the K beams, plus the (weighted) number, say M_{ON}, of trimming units, i.e.:

$$X = \sum_{k=1}^{K} \left(\sum_{n=1}^{4} |A_{\text{TTDU}}(k,n) - A_{\text{TCH}}(n)| \right) + \alpha M_{\text{ON}} \qquad (16)$$

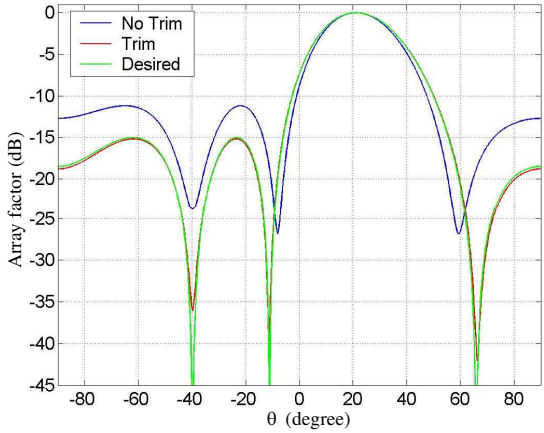

Figure 11. Comparison among the desired array factor and the one obtained with and without compensation: $\theta = 20^\circ$ ($\tau_{\max} = 90\,\text{ps}$).

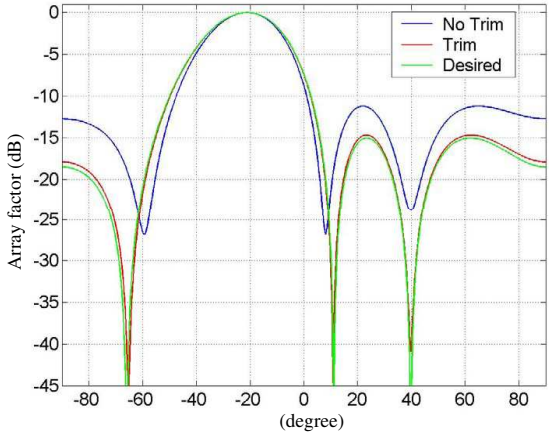

Figure 12. Comparison among the desired array factor and the one obtained with and without compensation: $\theta = -20^\circ$ ($\tau_{\max} = 90\,\text{ps}$).

A_{TTDU} being the excitation coefficients provided by the TTDU, (depending on the beam pointing configuration), A_{TCH} the Tchebitchev amplitude coefficients, K the number of the beams and α a penalty factor. It must be noted that the first term in Eq. (16) accounts for the trim compensation effect while the second term accounts for the hardware complexity of the trimming system.

The evolutionary algorithm minimizing the objective functional

is based on an iterative process made of three steps: selection, recombination and mutation. In particular, we used a tournament selection operator, an extended intermediate recombination process and a Gaussian mutation procedure [38].

The life cycle is repeated until the best fitness does not reach a certain minimum or until a specified number of iterations N_{it} is obtained.

The nominal Tchebitchev array factor, the array factor obtained with and without the compensation are reported in Figs. 10–14 for the five considered beam pointing angles, respectively. The trimming amounts obtained for all the trimming units are reported in Fig. 15. The evolutionary algorithm also allows to reduce the number of the trimming unit and, in the considered example allows to obtain a far-field pattern quite similar to the desired one by using only 6 trimming units.

8. A DIFFERENCE BEAM OTSA

In navigation systems and tracking radars, employed in military and civilian applications such as the weapon control, missile guidance, target tracking, precision landing, air traffic, ships and automotive control [39, 40] the availability of antenna systems radiating both sum and difference patterns is of great interest.

Generally speaking, the radar antenna systems have to guarantee

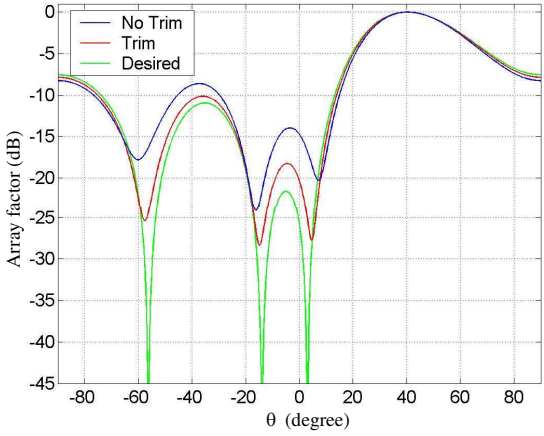

Figure 13. Comparison among the desired array factor and the one obtained with and without compensation: $\theta = 40^{\circ}$ ($\tau_{\max} = 90\,\mathrm{ps}$).

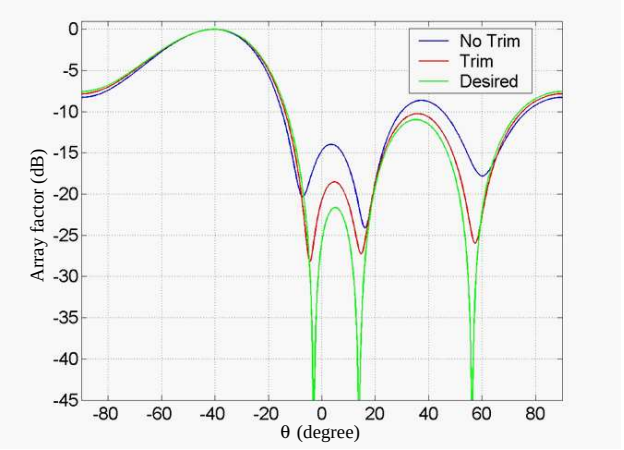

Figure 14. Comparison among the desired array factor and the one obtained with and without compensation: $\theta = -40^\circ$ ($\tau_{\max} = 90\,\text{ps}$).

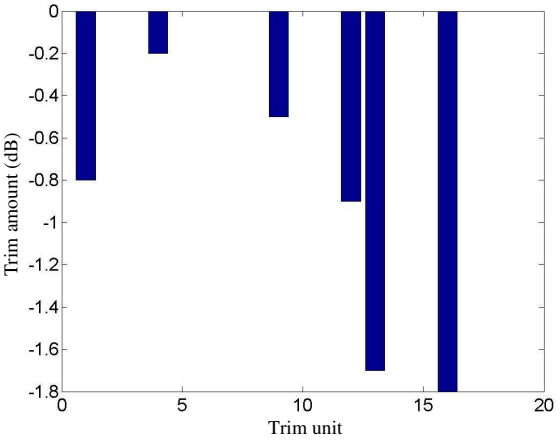

Figure 15. Trim amounts to be applied for each of the 20 trim devices ($\tau_{\max} = 90\,\text{ps}$).

the electronic beam steering control, a high angle and range resolution, multiple beams and, often, an independent control of the shape of the sum and difference patterns.

Usually, to achieve accurate tracking systems, the monopulse technique is adopted [40] wherein the antenna system radiate a sum pattern and two difference patterns for azimuth and elevation angular tracking.

Moreover, in these applications, wideband systems are of interest, since ultra-wide band radars allow better range measurement accuracy and range resolution, target recognition, improved radar immunity to passive interferences and improved target tracking stability [41].

In this section, we present an optical BFN architecture providing wide band, beam-squint free, applied to generate sum and difference patterns.

The basic idea is to exploit the available results on the phase and time control techniques [3] wherein the optical phase control is achieved by referring to a coherent detection scheme, and the time control exploits a direct detection one.

Wide band sum patterns are realized by using a proper time delay distribution while for a wide band difference pattern, an additional phase shift of π between the contributions from the two halves of the array is required.

Obviously, to guarantee the wide band behaviour, the phase opposition term must be constant across the whole system bandwidth.

In the following, to control the phase opposition term we propose an optical BFN based on the coherent detection scheme, the Heterodyne Phaser (HP), proposed in [42], in principle, able to provide a differential phase shift constant across a large bandwidth [43].

Let us consider the optically controlled heterodyne phaser scheme reported in [42] (Fig. 16).

The laser source with optical frequency ω_0 and amplitude A_0 is equally subdivided between the two interferometer arms. In the upper arm an Optical Frequency Shifter (OFS) enforces a frequency shift equal to the RF frequency ω_{RF}. In the lower arm an optical phase shifter (OPS) controls the optical phase by adding a variable phase shift equal to φ. The two light signals, after combining, feed the photodetector. Accordingly, the output current i_{PD} of the photodetector will contain the term:

$$i_{PD} \propto \frac{A_0^2}{2} \cos(\omega_{\mathrm{RF}} t + \omega_{\mathrm{RF}} \tau_0 - \varphi) \tag{17}$$

where τ_0 represents a constant delay corresponding to the output delay lines. Since the variable phase shift φ is independent from the RF frequency, a differential phase shift constant across the phaser bandwidth can be set among two or more radiating elements.

The HP bandwidth depends mainly on the spectral properties of the OFS. Optical frequency shifters are discussed in [44, 45] while optical controlled phase shifters are described in [46–48]; the wide band operation has been demonstrated over a 2 to 18 GHz bandwidth in [48] and an extension of such a structure up to 40 GHz is under study.

It is worth noting that the heterodyne phaser can also be obtained by using a two lasers scheme: the two lasers provide the frequency shifted light signals thus avoiding the use of the OFS. However, when adopting two beat lasers, the phase noise of each laser contributes to the phase noise of the beat microwave signal, thus widening the detected signal linewidth [49]. Accordingly, to generate high quality microwave signals it is necessary to properly establish a phase coherence between the two lasers [49, 50].

The architecture we propose to realize sum and difference wide band patterns, exploiting both HP and optical time shifters, is reported in Fig. 17 wherein the array of N elements appears subdivided into two parts. The two arrays are driven by means of an optical time shifter in order to allow a wideband beam squint free beamsteering, while two HP's control the proper phase term needed to achieve a sum or a difference patterns. In Fig. 17 the phase terms are set in order to get a phase opposition as required in difference patterns.

This architecture allows to compensate for systematic phase errors, introduced by the HP, among the two halves of the array. Moreover, it could be possible to integrate the HP's and the TTD phaser in order to achieve a fully integrated compact BFN.

The architecture has been tested by considering a 8 elements array, with a half a wavelength spacing, at 20 GHz, and simulating the whole structure using the BFN models described in Section 6. The HP has been modelled by using an ideal OFS and OPS, since we are not interested here on the real system bandwidth, but only in proving the architecture capabilities. A TTDU working in the 3 bits — 4 elements configuration has been considered as time steering unit, so that each half array is driven by a single TTDU. No trimming units have been introduced.

The amplitude of the array factor has been evaluated as a function of the frequency of the RF signal and the observation angle θ. The case of a difference beam pointing at the angle $\theta = -10^\circ$ is shown in

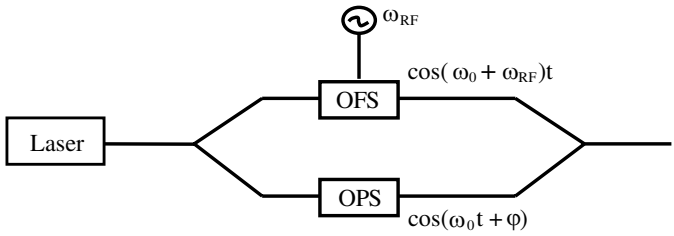

Figure 16. Scheme of the HP.

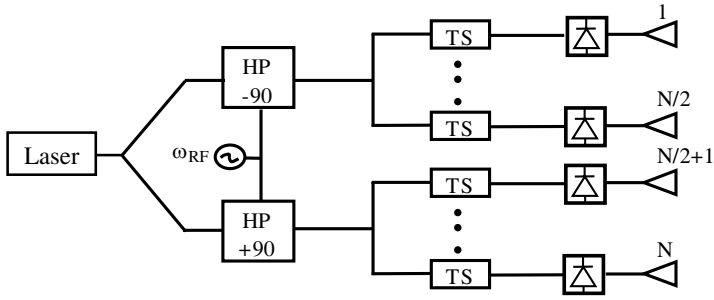

Figure 17. Scheme of the optical architecture proposed to realize both wide band sum and difference pattern: In the graph the HPs are set in order to get a difference pattern.

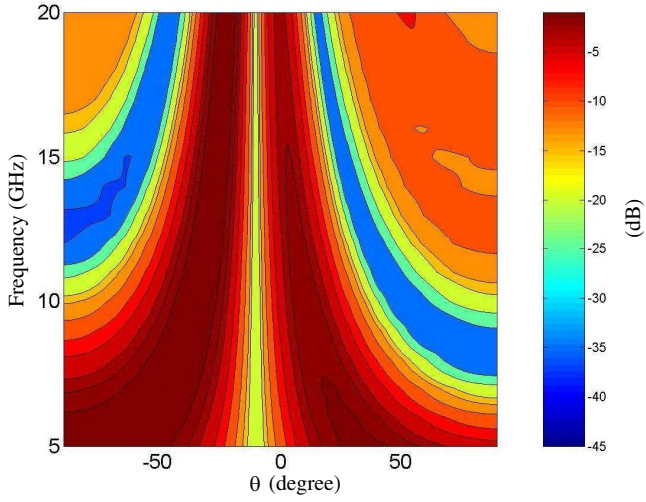

Figure 18. Array factor intensity plot as function of the angle θ and the frequency of the MW signal: Difference beam squint free pattern pointing towards $\theta = -10°$.

Fig. 18, for a frequency range from 8 to 20 GHz. The results show that the null pointing is not subjected to the frequency squint. However, as in the cases reported in the previous sections, due to the losses inside the TTDU, the pattern shape deteriorates as the beam pointing angle grows. Obviously, this effect observable in Fig. 18, can be compensated exploiting the strategy shown in Section 7.

9. CONCLUSIONS

The potentialities of an integrated optical TTD unit for beam squint free phased array antennas have been presented. In particular, the design of an OTSA based on this unit has been discussed, by considering different working configurations, and the antenna performance evaluated.

To make effective the OTSA design, taking into account for the mutual coupling issues, and the presence of the random, periodic and systematic errors on the antenna excitations distribution, its behavior has been realistically simulated thanks to a tool realizing the synergy between an optical and an RF CAD. In particular, regarding the compensation of the effects of the systematic errors, a proper trimming strategy has been developed and tested by using the mentioned tool.

Finally, an all optical architecture providing difference beam squint free patterns has been proposed.

Regarding the time delay unit, it realizes a SDL matrix and works analogously to a parallel delay line. A detailed comparative analysis is presented in [25].

REFERENCES

1. Fourikis, N., *Phased Array Based Systems and Applications*, Wiley-Interscience, 1997.
2. Mailloux, R. J., *Phased Array Antenna Handbook*, Artech House, Norwood, MA, 2005.
3. Riza, N. A., *Selected Papers on Photonic Control Systems for Phased Array Antennas*, Spie Milestone Series, 1997.
4. Zmuda, H. and E. N. Toughlian, *Photonic Aspects of Modern Radar*, Artech House, Norwood, MA, 1997.
5. Frigyes, I. and A. J. Seeds, "Optically generated true-time delay in phased-array antennas," *IEEE Trans. Microwave Theory Tech.*, Vol. 43, No. 9, 2378–2386, Sept. 1995.
6. Bratchikov, A. N., "Optical beamforming technology for active phased array," *Millennium Conference on Antennas & Propagation Antennas*, Davos, Switzerland, Apr. 9–14, 2000.
7. Matthews, P. J., "Photonics for phased array systems," *IEEE International Conference on Phased Array Systems and Technology*, 349–352, May 21–25, 2000.
8. Matthews, P. J., "Practical photonic beamforming," *International Topical Meeting on Microwave Photonics*, Vol. 1, 271–274, Nov. 17–19, 1999.

9. Nirmalathas, A., D. Novak, R. Waterhouse, and C. Lim, "Photonics as an enabling technology for future microwave systems," *Asia-Pacific Microwave Conference*, 912–916, Dec. 3–6, 2000.
10. Goutzoulis, A. P., D. K. Davies, and J. M. Zomp, "Prototype binary fiber optic delay line," *Optical Engineering*, Vol. 28, No. 11, 1193–1202, 1989.
11. Ng, W., A. A. Walston, G. L. Tangonan, J. J. Lee, I. L. Newberg, and N. Bernstein, "The first demonstration of an optically steered microwave phased array antenna using true-time-delay," *Journal of Lightwave Technology*, Vol. 9, No. 8, 1124–1131, 1991.
12. Soref, R., "Optical dispersion technique for time-delay beam steering," *Applied Optics*, Vol. 31, 7395–7397, 1992.
13. Esman, R. D., et al., "Fiber-optic prism true time-delay antenna feed," *IEEE Photon. Technol. Lett.*, Vol. 5, No. 11, 1247–1249, 1993.
14. Roman, J. E., M. Y. Frankel, P. J. Matthews, and R. D. Esman, "Time steered array with a chirped grating beamformer," *Electronics Letters*, Vol. 33, No. 8, 652–653, 1997.
15. Frankel, M. Y., P. J. Matthews, and R. D. Esman, "Two dimensional fiber optic control of a true time-steered array transmitter," *IEEE Trans. Microwave Theory Tech.*, Vol. 44, No. 11, 2696–2702, 1996.
16. Frankel, M. Y., P. J. Matthews, and R. D. Esman, "Wideband array transmitter with two dimensional fiber optic beam steering," *IEEE Intern. Symp. on Phased Array Systems and Technology*, 425–428, Oct. 15–18, 1996.
17. Yegnanarayanan, S., P. D. Trinh, and B. Jalali, "Recirculating photonic filter: A wavelength selective time delay for phased array antennas and wavelength code-division multiple access," *Optics Lett.*, Vol. 21, No. 9, 740–742, 1996.
18. Jung, B. M., J. D. Shin, and B. G. Kim, "Optical true time-delay for two-dimensional X-band phased array antennas," *IEEE Photon. Techol. Lett.*, Vol. 19, No. 12, 877–879, 2007.
19. Subbaraman, H., M. Y. Chen, and R. T. Chen, "Photonic crystal fiber-based true-time-delay beamformer for multiple RF beam transmission and reception of an X-band phased-array antenna," *Journal of Lightwave Technology*, Vol. 26, No. 15, 2803–2809, 2008.
20. Morton, P. A. and J. B. Khurgin, "Microwave photonic delay line with separate tuning of the optical carrier," *IEEE Photon. Techol.*

Lett., Vol. 21, No. 22, 1686–1688, 2009.

21. Barmenkov, Y. O., J. L. Cruz, A. Díez, and M. V. Andrés, "Electrically tunable photonic true-time-delay line," *Optics Express*, Vol. 18, No. 17, 17859–17864, 2010.
22. Khan, S., M. A. Baghban, and S. Fathpour, "Electronically tunable silicon photonic delay lines," *Optics Express*, Vol. 19, No. 12, 11780–11785, 2011.
23. Marpaung, D., et al., "Towards a broadband and squint-free Ku-band phased array antenna system for airborne satellite communications," *5th European Conference on Antennas and Propagation, (EUCAP)*, 2623–2627, Rome, Italy, Apr. 11–15, 2011.
24. Curcio, C., "Photonic wideband phased array: An optical time steered antenna based on a new true time delay unit," Ph.D. Thesis, 224, Jun. 2006.
25. Capozzoli, A., C. Curcio, and G. D'Elia, "A flexible integrated photonic true time delay phaser for phased array antennas," *Progress In Electromagnetics Research B*, Vol. 38, 261–279, 2012.
26. Goutzoulis, A. P. and D. K. Davies, "Hardware compressive 2D fiber optic delay line architecture for time steering of phased array," *Applied Optics*, Vol. 29, No. 36, 5353–5359, 1990.
27. Jespersen, N. V. and P. R. Herczfeld, "Phased array antennas with phasers and true time delay phase shifters," *Antennas and Propagation Society Symposium*, Vol. 2, 778–781, May 7–11, 1990.
28. Fouquet, J. E., "Compact optical cross-connect switch based on total internal reflection in a fluid-containing planar lightwave circuit," *OFC*, Vol. 1, 204–206, Mar. 7–10, 2000.
29. Fouquet, J. E., S. Venkatesh, M. Troll, D. Chen, H. F. Wong, and P. W. Barth, "A compact, scalable cross-connect switch using total internal reflection due to thermally-generated bubbles," *Annual Meeting of the IEEE Lasers and Electro-Optics Society*, Vol. 2, 169–170, Dec. 1–4, 1998.
30. Venkatesh, S., et al., "Performance improvements in bubble-actuated photonic cross-connect switches," *Annual Meeting of the IEEE Lasers and Electro-Optics Society*, Vol. 1, 39–40, Nov. 10–14, 2002.
31. Milligan, A. T., *Modern Antenna Design*, Wiley-IEEE Press, 2005.
32. Bucci, O. M., A. Capozzoli, G. Chiaretti, C. Curcio, G. D'Elia, and A. Fincato, "An integrated photonic true time delay unit for phased array antennas," *Atti della XV RiNEM*, 277–280, Cagliari,

Sept. 13–16, 2004.

33. Derickson, D., Editor, *Fiber Optic Test and Measurements*, Prentice Hall, New Jersey, 1998.
34. Harres, D. N., "Using statistical methods to predict link quality in COTS-based fiber optic networks," *20th Conference Digital Avionics Systems*, Vol. 1, 4D3/1–4D3/8, Oct. 14–18, 2001.
35. Herrmann, J. J. and K. W. Murphy, "Statistical optical analysis of passive optical networks provides 'plug and play' installation with fiber in the loop system," *5th Conference on Optical/Hybrid Access Networks*, 3.04/01–3.04/06, Sept. 7–9, 1993.
36. Uhing, J., S. Thomas, and C. Christodoulou, "A statistical approach for estimating the loss contribution of concatenated connectors in fiber-optic links," *National IEEE Aerospace and Electronics Conference*, Vol. 1, 239–245, May 21–25, 1990.
37. Lo, Y. T. and S. W. Lee, *Antenna Handbook — Theory, Applications and Design*, Chapter 18 by R. Tang, Practical Aspect of Phased Array Design, Van Nostrand Reinhold Company, New York, 1988.
38. Back, T., D. B. Fogel, and Z. Michalewicz, *Handbook of Evolutionary Computation*, Institute of Physics Publishing and Oxford University Press, 1997.
39. Chyba, M., "Planar array antenna for secondary radar synthesis," *International Conference on Microwaves, Radar and Wireless Communications*, Vol. 1, 174–177, May 22–24, 2000.
40. Skolnik, M. I., *Radar Handbook*, McGraw Hill, 1970.
41. Immorev, I. J. and J. D. Taylor, "Future of radars," *IEEE Conference on Ultra Wideband Systems and Technologies*, 197–199, May 21–23, 2002.
42. Soref, R. A., "Voltage controlled optical/RF phase shifter," *Journal of Lightwave Technology*, Vol. 3, No. 5, 992–998, 1985.
43. Hietala, V. M., G. A. Vawter, W. J. Meyer, and S. H. Kravitz, "Phased-array antenna control by a monolithic photonic integrated circuit, optical technology for microwave applications," *Proc. SPIE*, V. S.-K. Yao, Editor, Vol. 1476, 170–175, 1991.
44. Jez, D. R., K. J. Cearns, and P. E. Jessop, "Optical waveguide components for beam forming in phased array antennas," *Microwave and Optical Technology Letters*, Vol. 15, No. 1, 46–49, 1997.
45. Matsumoto, K, M. Izutsu, and T. Sueta, "Microwave phase shifter using optical waveguide structure," *Journal of Lightwave Technology*, Vol. 9, No. 11, 1523–1527, 1991.

46. Coward, J. F., T. K. Yee, C. H. Chalfant, and P. H. Chang, "A photonic integrated-optic RF phase shifter for phased array antenna beam-forming applications," *Journal of Lightwave Technology*, Vol. 11, No. 11, 2201–2205, 1993.
47. Henion, S. R. and P. A. Schulz, "Electrooptic phased array transmitter," *IEEE Photon. Technol. Lett.*, Vol. 10, No. 3, 424–426, 1998.
48. Winnall, S. T., A. C. Lindsay, and G. A. Knight, "A wide-band microwave photonic phase and frequency shifter," *IEEE Trans. Microwave Theory Tech.*, Vol. 45, No. 6, 1003–1006, 1997.
49. Goldberg, L., R. D. Esman, and K. J. Williams, "Generation and control of microwave signals by optical techniques," *IEE Proceedings J. Optoelectronics*, Vol. 139, No. 4, 288–295, 1992.
50. Blanchflower, I. D. and A. J. Seeds, "Optical control of frequency and phase of GaAs MESFET oscillator," *Electron. Lett.*, Vol. 25, No. 5, 359–360, 1989.